LAWRENCE
LIVERMORE
NATIONAL
LABORATORY

LLNL-JRNL-561992

Spontaneously intermixed Al-Mg barriers enable corrosion-resistant Mg/SiC multilayer coatings

R. Soufli, E. T. Al

June 20, 2012

Applied Physics Letters

Disclaimer

This document was prepared as an account of work sponsored by an agency of the United States government. Neither the United States government nor Lawrence Livermore National Security, LLC, nor any of their employees makes any warranty, expressed or implied, or assumes any legal liability or responsibility for the accuracy, completeness, or usefulness of any information, apparatus, product, or process disclosed, or represents that its use would not infringe privately owned rights. Reference herein to any specific commercial product, process, or service by trade name, trademark, manufacturer, or otherwise does not necessarily constitute or imply its endorsement, recommendation, or favoring by the United States government or Lawrence Livermore National Security, LLC. The views and opinions of authors expressed herein do not necessarily state or reflect those of the United States government or Lawrence Livermore National Security, LLC, and shall not be used for advertising or product endorsement purposes.

Spontaneously intermixed Al-Mg barriers enable corrosion-resistant, high-performance Mg/SiC multilayer coatings for extreme ultraviolet wavelengths

Regina Soufli[1*], Mónica Fernández-Perea[1,2], Sherry L. Baker[1], Jeff C. Robinson[1], Jennifer Alameda[1], Christopher C. Walton[1]

[1]Lawrence Livermore National Laboratory, 7000 East Avenue, Livermore, CA 94550

[2]Consejo Superior de Investigaciones Científicas, C/ Serrano 144, 28006 Madrid, Spain

[Abstract]

Magnesium/silicon carbide (Mg/SiC) has the potential to be the best-performing reflective multilayer coating in the 25-80 nm wavelength region but suffers from Mg-related corrosion, an insidious problem which completely degrades reflectance. We have elucidated the origins and mechanisms of corrosion propagation within Mg/SiC multilayers. Based on our findings, we have demonstrated a novel, efficient and simple-to-implement corrosion barrier for Mg/SiC multilayers. The barrier consists of nanometer-scale Mg and Al layers that intermix spontaneously to form a partially amorphous Al-Mg layer and is shown to prevent atmospheric corrosion while maintaining the unique combination of favorable Mg/SiC reflective properties.

[Manuscript Text]

Multilayer interference coatings have revolutionized numerous science and technology fields by enabling efficient normal-incidence imaging in the extreme ultraviolet (EUV) / x-ray wavelength region. Magnesium/silicon carbide (Mg/SiC)[1,2] multilayers have a wealth of applications as reflective coatings in the 25-80 nm wavelength region: solar and plasma physics, spectroscopy, EUV tabletop lasers, high-resolution microscopy and femtosecond chemistry[3,4,5,6,7]. Mg/SiC multilayers operate at wavelengths longer than 25 nm (Mg 2p edge), where Mg absorption is low and the contrast between the refractive indices of the constituent Mg and SiC layers, combined with sharp and stable layer interfaces, produce peak reflectance of 30-50% at near-normal incidence angles. In addition to high reflectance, Mg/SiC possesses several other favorable properties: near-zero film stress, good spectral selectivity and thermal stability up to 350° C. This combination of superior properties is unmatched by any of the other candidate multilayer material pairs in the > 25 nm wavelength region such as Mo/Si, SiC/Si, Si/B_4C, Al/SiC and Sc/Si. However, the issue of corrosion has prevented Mg/SiC from being used in applications that require long-term stability. In the past 10 years, and based on its unparalleled optical performance, Mg/SiC has been selected as EUV mirror coating in telescopes for high-visibility scientific missions such as NASA's Solar Dynamics Observatory (SDO)[8]. But Mg/SiC corrosion ultimately led to the use of alternative coatings[9], resulting in a reduction of instrument light throughput by a factor of 10 and in increased coating stress. Mg/SiC is being considered again as mirror coating for future EUV solar missions[10,11], but its implementation is still hindered by the corrosion issue[11]. Although it is established that Mg is prone to corrosion upon atmospheric exposure, the specifics of the initiation and propagation of corrosion in nanometer-scale Mg/SiC

multilayer thin films have not been understood and no methods have been found to prevent it[11]. Mg is a material widely used in the automotive, aerospace and consumer product industries and various methods to mitigate corrosion in bulk Mg have been developed[12]. Nevertheless, nanometer-scale Mg/SiC reflective multilayer coatings for the EUV region have distinctly different physical properties and operational requirements, compared to their bulk Mg and SiC counterparts. Corrosion inhibitors for bulk Mg, Mg alloys and thick Mg films[12,13], such as oxides, organic/polymer layers and other compound materials, cannot be adopted for Mg/SiC multilayers because they have high absorption in the EUV and would reduce the Mg/SiC multilayer reflectance to near zero.

Mg/SiC films discussed in this paper were deposited in a planar DC-magnetron sputtering deposition system[14] located at Lawrence Livermore National Laboratory (LLNL). The base vacuum pressure in the deposition chamber was 10^{-8} Torr and argon (Ar) was used as process gas at 10^{-3} Torr. Temperature was maintained below 70° C during deposition. The quoted sputtering source (target) purity was 99.97 wt. % for Mg, 99.9999 wt. % for SiC and 99.9995 wt. % for Al. Sputtering targets were operated at 1200 W (Mg) and 2000 W (SiC, Al). After deposition, all samples were stored and handled under identical conditions, in ambient laboratory environment. The Scanning Electron Microscopy (SEM) images in Figs. 1, 3(a), 4(a) were obtained with a Leo 1560™ instrument at LLNL, operated at 3 kV voltage and equipped with a Gemini® field emission column and an in-lens annular detector. The images in Figs. 2(a), 2(b) and 3(b) were obtained at Evans Analytical Group (EAG) Labs (Sunnyvale, California) with an SEM instrument operated at 5 kV voltage and 0.4 nA current, part of the focused ion beam (FIB) dual-beam chamber (FEI Strata 400™) used for cross-section specimen preparation. The images in Figs 2(c), 2(d) and 3(c), 3(d), 3(e) were obtained at EAG Labs with a JEOL 2010

Transmission Electron Microscopy (TEM) instrument equipped with a 1 Mpixel camera. The images in Figs. 4(b), 4(c) were obtained at EAG Labs with an FEI Tecnai™ TEM instrument equipped with a 4 Mpixel camera. The thickness (in the direction perpendicular to the image plane) of the cross-section specimens shown in the TEM images in Figs. 2, 3 and 4 was estimated at 100 nm. X-ray Photoelectron Spectroscopy (XPS) measurements were performed at EAG Labs with a Physical Electronics Quantum 2000™ instrument, using an Al K_α (1,486.6 eV) x-ray source at a take-off angle of 90°. High-resolution XPS spectra were obtained at pass energies of 23.5 eV. The x-ray beam size (analysis area) on the sample was 1.4×0.3 mm^2 and the analysis depth range was 5-10 nm from the top surface. Large-angle X-ray diffraction (LAXRD) measurements were performed with a PANalytical X'Pert PRO MRD™ instrument using a Cu K_α (8,047.8 eV) x-ray source, in $\theta/2\theta$ geometry at step size (2θ) of 0.02°. The EUV reflectance measurements plotted in Fig. 5(a) and discussed throughout the manuscript were performed at the reflectometer facility at beamline 6.3.2.[15] of the Advanced Light Source (ALS) synchrotron at Lawrence Berkeley National Laboratory. An 80 lines/mm grating monochromator was used for wavelength selection. Wavelength calibration was based on the $L_{2,3}$ absorption edge of an Al transmission filter with a relative accuracy of 0.011% rms, and was determined with 0.007% repeatability. Second harmonic and stray light suppression was achieved with a Mg transmission filter. For third and higher-order harmonic suppression, an "order suppressor" based on the principle of total external reflection and consisting of three carbon mirrors at 20° grazing incidence angle was used in addition to the filters. The ALS storage ring current was used to normalize the signal against the storage ring current fluctuations. Signal was collected with a Si photodiode detector with an acceptance angle of 2.4 degrees. Reflectance was measured with a

relative accuracy of ± 0.5 %, determined by the photodiode uniformity in the wavelength range of the measurements.

Atmospheric corrosion in Mg/SiC multilayer films is caused by Mg interacting with environmental agents such as humidity and reactive ions[13,16]. Although the multilayer deposition process and the eventual EUV applications take place in vacuum environments, the Mg/SiC-coated mirrors inevitably have to be exposed to air for calibration, installation and alignment. Mg/SiC corrosion is exhibited as spots which sporadically and progressively emerge and expand across the coating over time. Fig. 1 shows detailed topography from a Mg/SiC multilayer aged for 3 years after deposition, with advanced corrosion visible to the eye. Fig. 2 shows in more detail the structure in one of the most severely corroded regions of the same sample. Regions with "cellular" appearance have formed in the corroded area where the inner Mg layers are exposed, Fig. 2(c), 2(d). Using XPS, summarized in Fig. 2(e), it was determined that in the corroded areas Mg is present entirely as a combination of $Mg(OH)_2$, $Mg(CO)_3$ and MgO[16]. This is consistent with previous literature on Mg corrosion, which reports voluminous and acicular corrosion products, a mixture of brucite [$Mg(OH)_2$] and hydromagnesite (a hydrated $Mg(CO)_3$ mineral)[17,18]. The erupting top sections of the multilayers shown in the SEM images in Figs. 1 and 2(a), 2(b) can be explained by volume expansion during the formation of the Mg corrosion products. Fig. 3(a) shows a multitude of corrosion spots from early, pre-eruptive stages of Mg/SiC corrosion, not visible by eye. Cross-sectional TEM was performed on one of these spots, Fig. 3(b), 3(c). A layer of Mg corrosion products, much thinner than the layer shown in the severely corroded sample in Fig. 2, has formed just underneath the top SiC layer. LAXRD measurements on multilayer areas affected by both early and advanced corrosion (as in Fig. 2(a)

and 3(a), respectively) showed a strong peak at detector angle $2\theta = 34.46° \pm 0.03°$ attributed to Mg (002)[19] and corresponding to 0.26 nm atomic spacing in the Mg crystal lattice, indicating strongly textured (002) orientation from the undisturbed Mg layers in the multilayer. Using the Scherrer equation, the Mg crystallite (grain) size in the direction perpendicular to the Si substrate was calculated to be 17.3 ± 0.3 nm, which is close to the Mg layer thickness in the multilayer after interdiffusion effects at the Mg-SiC layer interfaces are taken into account. Therefore, the Mg layer thickness appears to be the limiting factor in the Mg crystallite size. Other LAXRD peaks (lower by 2 to 3 orders of magnitude) from corroded areas at $2\theta = 31.07$, 44.48, 61.69, 72.69, 75.22, 76.32 and $78.02 \pm 0.03°$ were attributed to the presence of polycrystalline hydromagnesite in the corrosion products.

Figs. 1, 2 and 3 shed light on the origins and mechanisms of corrosion propagation in Mg/SiC multilayer structures. Provided that the substrate surface (such as the semiconductor-grade Si wafer substrates used in these experiments) is sufficiently clean, it is evident that corrosion attacks the multilayer film from the top surface at local entry points such as pinholes, particles and grain boundaries inherent in sputtered thin films. Other localized damage may also occur on the top surface after deposition and during handling of the samples, such as dents and scratches. Such defects act as preferential sites for dissociation and chemisorption and provide pathways for humidity and reactive ions present in the environment to reach the topmost Mg layers [13,20,21]. Earlier authors[11] have attributed the degradation of Mg/SiC multilayers and the presence of Mg at the top surface to inter-diffusion processes at the Mg and SiC layer interfaces. However, based on the experimental results and observations reported here, this does not appear to be the case. Although corrosion may not propagate all the way to the bottom of the multilayer stack, the thick

layer of corrosion products formed on top reduces the EUV reflectance to zero thus rendering the multilayer useless, as has been verified by EUV reflectance measurements on corroded Mg/SiC samples.

To address the corrosion problem we have developed barrier structures which nearly eliminate corrosion while maintaining all the favorable reflective properties of Mg/SiC multilayers. Such a corrosion-resistant Mg/SiC multilayer, aged for 3 years after deposition, is shown in Fig. 4. Fig. 4(a) shows one of the most corroded areas found on the multilayer. Comparison of Fig. 4(a) with Figs. 1, 2(a) and 3(a) demonstrates the dramatic reduction of corrosion in the new, corrosion-resistant multilayers. The corrosion-barrier layer is a 39 nm-thick layer consisting of 19 nm Mg and 20 nm Al sputtered as two consecutive layers, which spontaneously intermix to form a partially amorphous layer, as evidenced by comparing the morphology of the intermixed Al-Mg layer with the individual, crystalline Mg and Al layers shown in Figs. 4(b) and 4(c). The intermixed layer consists of sparse Al and Mg crystallites embedded in a matrix of amorphous Al-Mg material. The spontaneous intermixing and amorphization between the Al and Mg layers is reported in this work for the first time in the literature. Separate LAXRD measurements on the Al-Mg corrosion barrier layer, Fig. 4(d), 4(e), show that the amorphization process takes place over an extended period of time. Two days after deposition, the Al and Mg layers appear strongly textured in the Al (111) and Mg (002) orientations respectively and the crystallite sizes are nearly equal to the as-deposited Al and Mg layer thicknesses. Nine weeks after deposition, both Al and Mg peak intensities are reduced and peaks are broadened. The average crystallite size is reduced by 70% for Al and by 45% for Mg. No Mg_xAl_y phases, such as the equilibrium β and γ phases, were observed by LAXRD. The corrosion barrier was inserted underneath the SiC

capping layer to provide additional protection from exposure to air. We believe that the spontaneous intermixing and partial amorphization of the Al-Mg barrier layer are responsible for its protective ability. It has been shown[13,16,21] that amorphous films have better passivating properties than crystalline ones due to reduced grain boundaries, vacancies and defects and thus reduced permeability to humidity, oxygen (O^{2-}) and other reactive ions such as chlorine (Cl^{-}) which are found in airborne salts and are common initiators of corrosion in Mg. The spontaneous intermixing of the Mg and Al layers can be explained as a solid state amorphization (SSA) reaction, as seen in other binary systems at room temperature[22,23]. Conditions favoring SSA are high enthalpy of mixing and high diffusivity of one material in the other, with both quantities being quite modest in the Al-Mg system compared with other well-known systems exhibiting SSA. Based on these criteria, Al-Mg is a rather unlikely candidate for SSA. But SSA can still occur when the crystalline phases (competing with the amorphous) face a large energy barrier to nucleation[22]. Such a large energy barrier is likely in Al-Mg because the equilibrium β phase has a large unit cell and is known to appear in non-equilibrium samples only after substantial annealing[24]. Furthermore, the strain and disorder at the Al/Mg layer interface caused by the lattice mismatch (fcc/hcp) between the Al and Mg layers could be an additional mechanism facilitating SSA, as has also been reported in Ref. 23 for another fcc/hcp system (Ni/Ti). Additional SEM and TEM analysis showed that, when a corrosion spot does rarely occur in protected Mg/SiC multilayers, it remains localized at isolated entry points. Figure 5 shows measured and modeled[25] EUV reflectance from standard Mg/SiC and corrosion-resistant Mg/SiC multilayers. The Al layer thickness was optimized in each wavelength region to maximize Mg/SiC multilayer reflectance while providing adequate corrosion protection at the wavelength of operation. The relative transparency of Al in the entire 25-80 nm wavelength range is

extremely beneficial towards maintaining high reflectance. It should be noted that attempts to produce MgAl/SiC multilayers using a MgAl alloy sputtering target resulted in more rapid and significant multilayer corrosion than that observed in standard Mg/SiC. Alloy targets, due to their preparation methods, often contain oxygen and other gaseous impurities which can act as corrosion initiators. The spontaneously intermixed Al-Mg layer discussed in this manuscript, formed by consecutively sputtering Mg and Al layers from ultra-pure elemental targets, may therefore have superior passivating properties compared to an equivalent layer deposited by a MgAl alloy target. It should also be noted that the deposition technique and the number and thickness of all layers including the SiC capping layer in the aforementioned Mg/SiC multilayers, have been optimized to achieve maximum EUV reflectance and lowest stress on large-area optic surfaces. Attempting to improve the multilayer corrosion resistance by increasing for example the thickness of the SiC capping layer would lead to a reduction in peak EUV reflectance (due to SiC absorption), which may be severe depending on the SiC thickness and the wavelength of operation.

In summary, we demonstrate a novel Mg/SiC corrosion barrier that is inexpensive and straightforward to implement, is fully compatible with the optimized sputtering deposition techniques used for EUV multilayer coatings, and maintains all the favorable reflective properties of Mg/SiC multilayers. The corrosion-resistant Mg/SiC multilayers described here will enable implementation of Mg/SiC mirror coatings in science and technology fields that require long-term stability, overcoming the long-standing limitation imposed by corrosion until now.

[Acknowledgements]

Financial support for Mónica Fernández-Perea was provided in part by Ministerio de Educacion y Ciencia, Programa Nacional de Movilidad de Recursos Humanos del Plan nacional de I+D+I 2008-2011. This work was performed under the auspices of the U.S. Department of Energy by Lawrence Livermore National Laboratory under Contract No. DE-AC52-07NA27344 and funding was provided in part by LLNL's Laboratory Directed Research and Development Program. The contributions of Harry Kawayoshi, Jiafang Lu, Martin Izquierdo and Shannon Xia (Evans Analytical Labs, Sunnyvale, California) in the acquisition of the TEM images and XPS results is gratefully acknowledged. We thank Eric Gullikson (Lawrence Berkeley National Laboratory) for support with the EUV reflectance measurements.

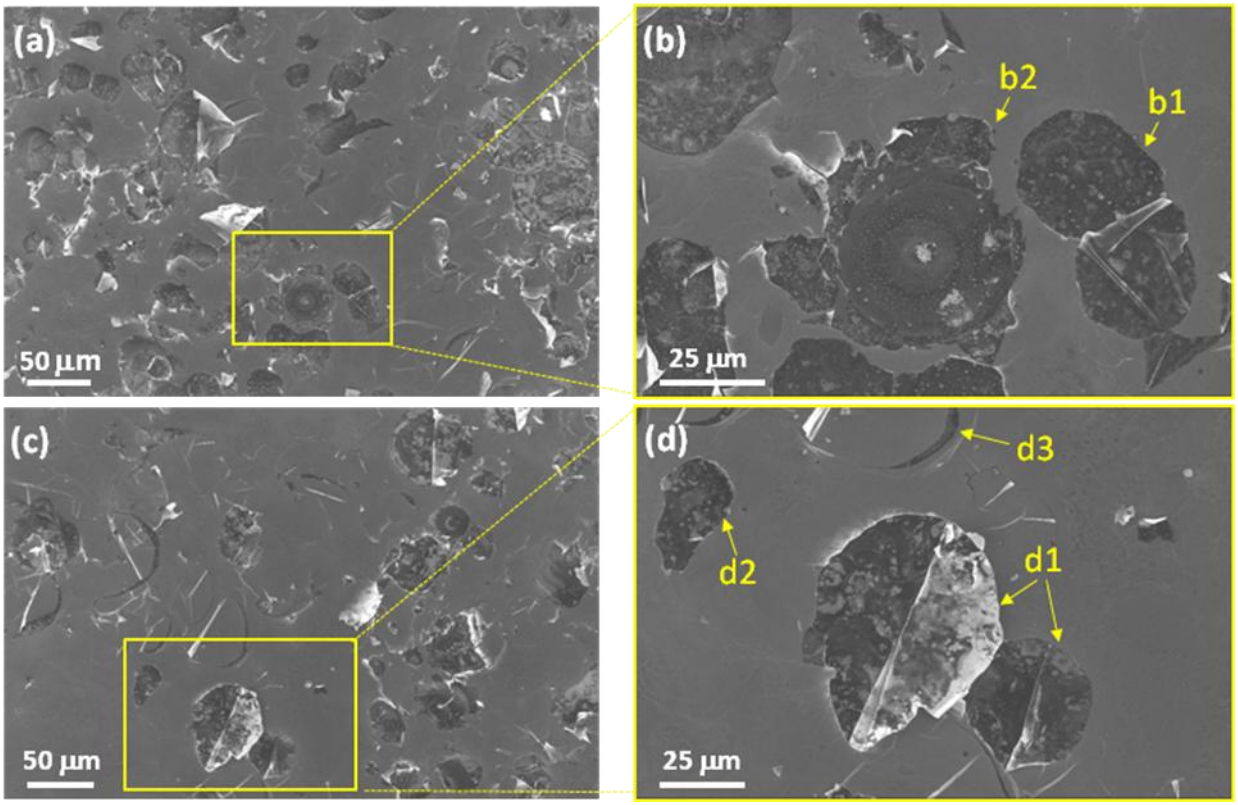

Fig. 1: SEM images of the top surface of severely corroded Mg/SiC multilayer films aged for 3 years. Frames (b), (d) are magnified views of selected areas from frames (a), (c) respectively. Some areas (d3) appear to be undergoing volume expansion and be ready to erupt. Other areas (b1, d1) have already erupted and are peeling off the top while still being partially attached to the surface. In other areas (b2, d2), the erupted sections of the multilayer have been removed from the top and are missing, thus exposing the inner layers. The as-designed multilayer structure of the depicted samples consists of a 100-mm diameter, 500-µm thickness Si (100) wafer substrate, coated with a film of total thickness $d_{total} = \{(d_{SiC,\ base} + [20 \times (d_{SiC} + d_{Mg})] + d_{SiC,\ top}]\} = 512$ nm, where $d_{SiC,\ base} = 3$ nm is the thickness of a bottom SiC layer, followed by a periodic multilayer structure consisting of N=20 Mg/SiC bilayers (periods) with period thickness $d_{SiC} + d_{Mg} = 6$ nm + 19 nm = 25 nm, followed by a top SiC capping layer with thickness $d_{SiC,\ top} = 9$ nm. The

multilayer was designed to have its peak reflectance at wavelength λ = 46.3 nm at θ = 85 degrees (near-normal) incidence angle.

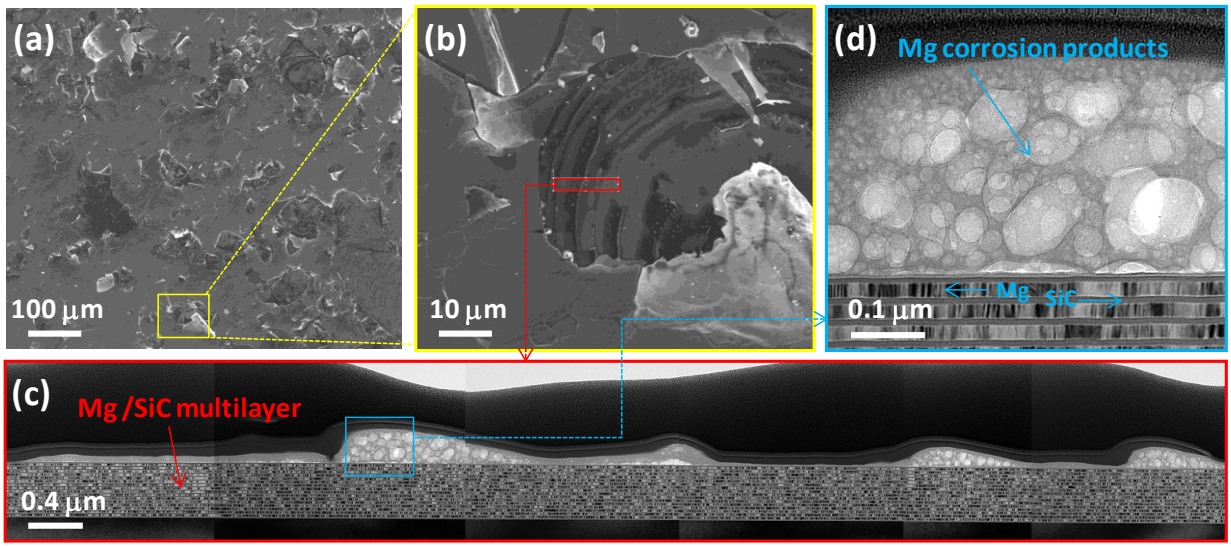

(e)

Binding energy (eV)	Orbital	Species
50.8	Mg 2p	MgO, $Mg(OH)_2$, $Mg(CO)_3$
532.8	O 1s	OH^-, $Mg(OH)_2$

Fig. 2: Images of a severely corroded region from a Mg/SiC multilayer film aged for 3 years. The multilayer design parameters of this sample are the same as described in the caption of Fig. 1. (a) SEM image of top surface. (b) Magnified view of detail from (a), showing the top portion of the film being delaminated and inner layers being exposed. The rectangle indicates the area (within the region of exposed inner layers) that was used for cross-sectional TEM. (c) Cross-sectional TEM image of corroded multilayer region. The 4 topmost Mg/SiC bilayers (out of the N=20 initially deposited bilayers) and the SiC capping layer have been consumed by corrosion and are missing from the entire TEM section of the multilayer. (d) Detail from (c) at higher magnification, showing undisturbed Mg (polycrystalline) and SiC (amorphous) layers and Mg

corrosion products appearing as a cellular structure on top. (e) XPS analysis results of corroded region on top surface. XPS peak assignments are based on Ref. 16.

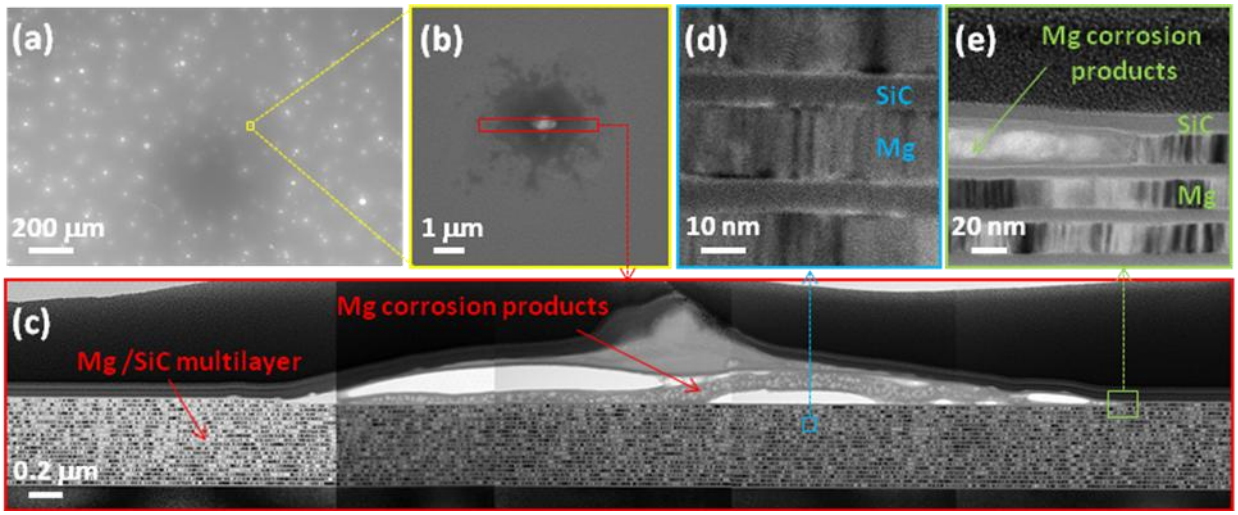

Fig. 3: Images of a region with initial stages of corrosion from a Mg/SiC multilayer film aged for 3 years. The multilayer design parameters of this sample are the same as described in the caption of Fig. 1. (a) SEM image of top surface. An average of 192 corrosion spots/mm^2 covering 46% of the Mg/SiC multilayer area was estimated. (b) Magnified view of corrosion spot from (a). The rectangle indicates the area that was used for cross-sectional TEM. (c) Cross-sectional TEM image of multilayer corroded spot. In the region where Mg corrosion products have formed, the topmost Mg layer and the SiC capping layer have been consumed by corrosion and are missing. (d) Detail from (c) at higher magnification, showing undisturbed Mg and SiC layers. (e) Detail from (c) at higher magnification, showing the advance and boundary of corrosion along the topmost Mg layer, underneath the SiC capping layer. A portion of the topmost Mg layer is already converted to corrosion products, while the rest of the Mg layer is intact.

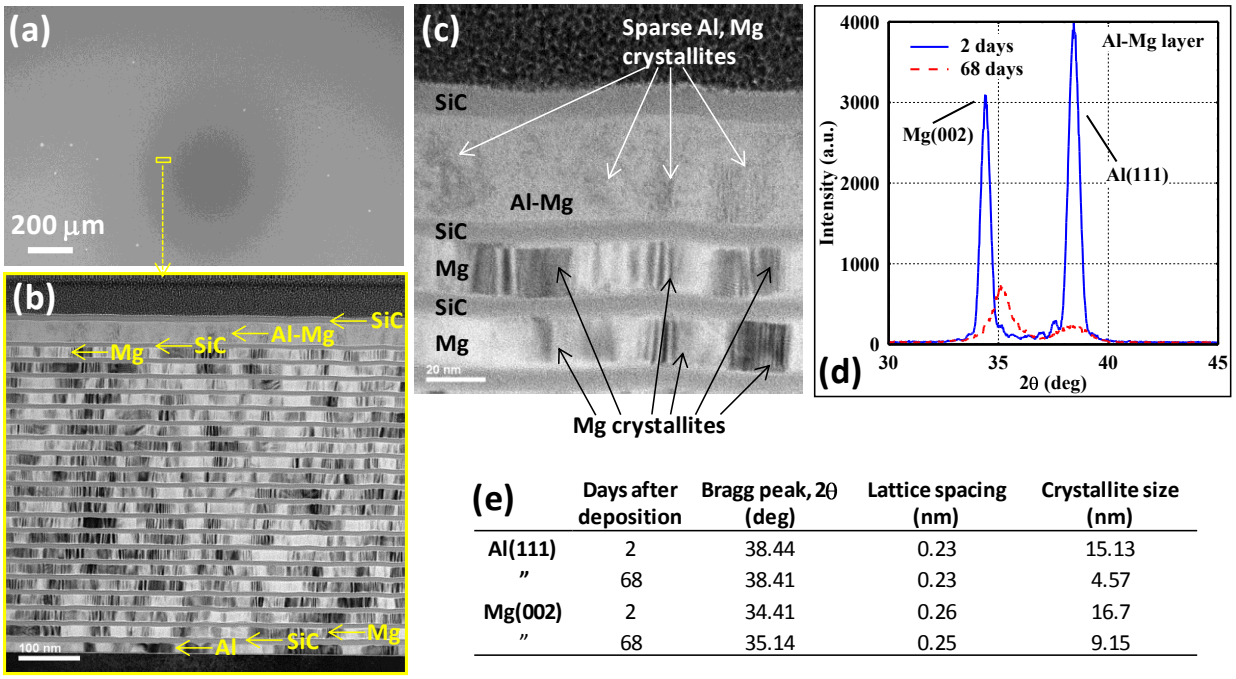

(e)

	Days after deposition	Bragg peak, 2θ (deg)	Lattice spacing (nm)	Crystallite size (nm)
Al(111)	2	38.44	0.23	15.13
”	68	38.41	0.23	4.57
Mg(002)	2	34.41	0.26	16.7
”	68	35.14	0.25	9.15

Fig. 4: Images from a corrosion-resistant Mg/SiC multilayer film aged for 3 years. (a) SEM image of top surface. A comparison with Figs. 1, 2(a) (standard Mg/SiC with advanced corrosion having completely destroyed the multilayer reflectance) and Fig. 3(a) (standard Mg/SiC with 192 corrosion spots/mm^2 covering 46% of the multilayer area) demonstrates the dramatic reduction of corrosion in the new, corrosion-resistant Mg/SiC. An average of 11 spots/mm^2 covering 0.07% of the multilayer area was estimated for corrosion-resistant Mg/SiC. (b) Cross-sectional TEM image of multilayer. It consists of the same structure described in the caption of Fig. 1, with the addition of (i) a 20 nm-thick Al layer above the topmost Mg layer and (ii) another 20 nm-thick Al layer inserted at the bottom of the multilayer on top of the Si substrate. The top Al layer intermixes spontaneously with the top Mg layer to form a partially amorphous Al-Mg layer which acts as the primary corrosion barrier. (c) Cross-sectional TEM image of the same multilayer sample at higher magnification, showing the top layers in the multilayer including the Al-Mg corrosion barrier layer. (d) LAXRD measurements of the Al-Mg layer obtained 2 and 68

days after deposition. (e) Calculated values for the Al and Mg lattice spacing (via the Bragg equation) and crystallite sizes (via the Scherrer equation) from the LAXRD measurements in (d). The Al (111) and Mg (002) peaks coincide with the tabulated values[19], except for the Mg (002) peak measured 68 days after deposition. A possible explanation for the Mg (002) peak shift towards longer angles could be the substitution of Al in the Mg lattice.

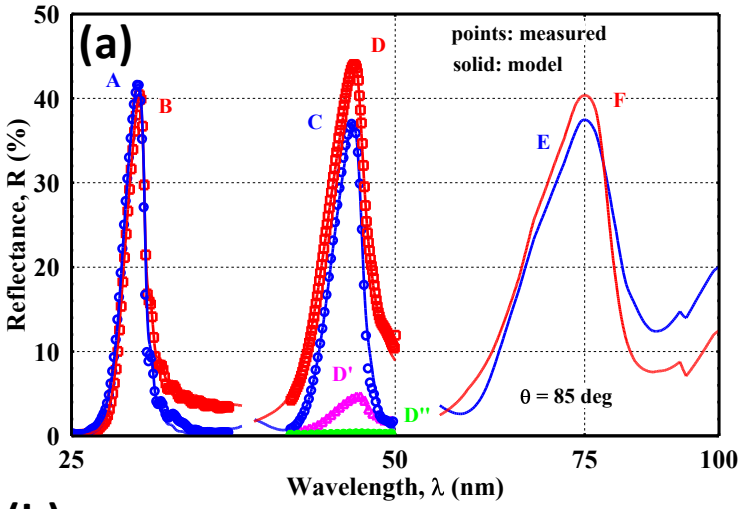

(b)

	A	B	C	D	D'	D''	E	F
λ_{peak} (nm)	28.9	28.9	45.7	45.7	46.2	46.4	75	75
R_{peak}(%)	42	40.5	37	44	4.6	0.22	37.5	40.4
$d_{Al, base}$ (nm)	12.7	-	26	-	-	-	20	-
$d_{Al, top}$ (nm)	12.7	-	26	-	-	-	10	-
N	35	35	20	20	20	20	10	10
d_{Mg} (nm)	9.9	9.8	18.9	18.1	18.1	18.1	34.8	38.6
d_{SiC} (nm)	5.1	5.1	6.9	7.1	7.1	7.1	14.9	12.9
$d_{SiC, base}$ (nm)	3	3	3	3	3	3	-	-
$d_{SiC, top}$ (nm)	9	9	9	9	9	9	9	9

Fig. 5: Reflective performance of corrosion-resistant and standard Mg/SiC multilayer coatings. (a) Measured and modeled EUV reflectance (1st order multilayer peaks) of corrosion-resistant (curves A and C) and standard (curves B, D, D' and D'') Mg/SiC multilayers optimized for operation at 28.9 and 45.7 nm wavelengths. Curves A, B, C and D were measured a few days after deposition. Curves D', D'' were obtained from the same multilayer sample as D, measured 3.5 years after deposition with corrosion present and illustrate the destructive effect of corrosion on Mg/SiC multilayer reflectance. A calculated design concept is also shown for corrosion-resistant (curve E) and standard (curve F) Mg/SiC multilayers optimized for operation at 75 nm. Here for the first time Mg/SiC multilayer coatings are proposed for operation in the 75 nm

wavelength region. The IMD software[25] was used for the modeling of multilayer performance, with experimental optical constants (refractive index) values obtained from Ref. 26 for Mg, Ref. 27 for SiC and Ref. 28 for Al. (b) Multilayer design parameters of the Mg/SiC coatings A-F shown in (a). The thickness d of all layers and number N of Mg/SiC bilayers is shown, together with the peak wavelength λ_{peak} and peak reflectance R_{peak} of each coating.

References

[1] H. Takenaka, S. Ichimaru, T. Ohchi, and E. M. Gullikson, *J. Electron Spectrosc. Relat. Phenom.* **144-147**, 1047 (2005).

[2] A. Aquila, F. Salmassi, Y. Liu, and E. M. Gullikson, *Optics Express* **17**, 22102 (2009).

[3] B. De Pontieu, S. W. McIntosh, M. Carlsson, V. H. Hansteen, T. D. Tarbell, P. Boerner, J. Martinez-Sykora, C. J. Schrijver, and A. M. Title, *Science* **331,** 55 (2011).

[4] N. Dudovich, O. Smirnova, J. Levesque, Y. Mairesse, M. Yu. Ivanov, D. M. Villeneuve, and P. B. Corkum, *Nature Phys.* **2,** 781 (2006).

[5] R. A. Bartels, A. Paul, H. Green, H. C. Kapteyn, M. M. Murnane, S. Backus, I. P. Christov, Y. Liu, D. Attwood, and C. Jacobsen, *Science* **297,** 376 (2002).

[6] B. R. Benware, C. D. Macchietto, C. H. Moreno, and J. J. Rocca, *Phys. Rev. Lett.* **81,** 5804 (1998).

[7] C. A. Brewer, A. Paul, H. Green, H. C. Kapteyn, M. M. Murnane, S. Backus, I. P. Christov, Y. Liu, D. Attwood, and C. Jacobsen, *Optics Letters* **33,** 518 (2008).

[8] R. Soufli, D. L. Windt, J. C. Robinson, S. L. Baker, E. A. Spiller, F. J. Dollar, A. L. Aquila, E. M. Gullikson, B. Kjornrattanawanich, J. F. Seely, and L. Golub, *Proc. SPIE* **5901,** 59010M (2005).

[9] P. Boerner, C. Edwards, J. Lemen, A. Rausch, C. Schrijver, R. Shine, L. Shing, R. Stern, T. Tarbell, A. Title, C. Jacob Wolfson, R. Soufli, E. Spiller, E. Gullikson, D. McKenzie · D. Windt, L. Golub, W. Podgorski, P. Testa, and M. Weber, *Solar Physics* **275,** 41 (2012).

[10] D. Martínez-Galarce, P. Boerner, R. Soufli, B. De Pontieu, N. Katz, A. Title, E. M. Gullikson, J. C. Robinson, and S. L. Baker, *Proc. SPIE* **7011,** 70113K (2008).

[11] M. G. Pelizzo, A. J. Corso, P. Zuppella, P. Nicolosi, S. Fineschi, J. Seely, B. Kjornrattanawanich, and D. L. Windt, *Opt. Eng.* **51**, 023801 (2012).

[12] J. E. Gray and B. J. Luan, *Alloys and Compounds* **336,** 88 (2002).

[13] E. McCafferty, *Introduction to Corrosion Science* (Springer, 2010).

[14] R. Soufli, R. M. Hudyma, E. Spiller, E. M. Gullikson, M. A. Schmidt, J. C. Robinson, S. L. Baker, C. C. Walton, and J. S. Taylor, *Appl. Opt.* **46,** 3736 (2007).

[15] J. H. Underwood and E. M. Gullikson, *J.Electr. Spectr. Rel. Phenom.* **92**, 265 (1998).

[16] H. B Yao, Y. Li, and A. T. S. Wee, *Appl. Surf. Sci.* **158,** 112 (2000).

[17] J. H. Nordlien, S. Ono, N. Masuko, and K. Nişancioğlu, *J. Electrochem Soc.* **142,** 3320 (1995).

[18] I. Nakatsugawa, S. Kamado, Y. Kojima, R. Ninomiya, and K. Kubota, *Corrosion Reviews* **16,** 139 (1998).

[19] Institute of Experimental Mineralogy, Russian Academy of Sciences http://database.iem.ac.ru/mincryst/search.php

[20] S. J. Splinter, N. S. McIntyre, W. N. Lennard, K. Griffiths, and G. Palumbo, *Surface Science* **292,** 130 (1993).

[21] P.L. Miller, B. A. Shaw, R. G. Wendt, and W. C. Moshier, *Corrosion Science* **51,** 922 (1995).

[22] R. B. Schwarz and W. L. Johnson, *Phys. Rev. Lett.* **51** 415 (1983).

[23] A.F. Jankowski, P. Sandoval, and J.P. Hayes, *Nanostructured Materials* **5,** 497 (1995).

[24] N. Al-Aqeeli, G. Mendoza-Suarez, and R. A. L. Drew, *Rev. Adv. Mater. Sci.* **18,** 231 (2008).

[25] D. L. Windt, *Computers in Physics* **12,** 360 (1998).

[26] M. Vidal-Dasilva, A. L. Aquila, E. M. Gullikson, F. Salmassi, and J. I. Larruquert, *J. Appl. Phys.* **108,** 063517 (2010).

[27] J. B. Kortright and D. L. Windt, *Appl. Opt.* **27,** 2841 (1988).

[28] E. Shiles, T. Sasaki, M. Inokuti, and D. Y. Smith, *Phys. Rev. B* **22,** 1612 (1980).